ADVANCED OPTICAL MATERIALS
www.advopticalmat.de

Materials Views
www.MaterialsViews.com

Performance Boost of Organic Light-Emitting Diodes with Plasmonic Nanostars

*Battulga Munkhbat, Hannes Pöhl, Patrick Denk, Thomas Arno Klar, Markus Clark Scharber, and Calin Hrelescu**

The performance of organic light-emitting diodes (OLEDs) is boosted by adding star-shaped plasmonic particles, so called nanostars. For this purpose, silver-enhanced gold nanostars coated with a thin silica shell, which tightly follow the nanostar morphology, are synthesized. An optimal spectral overlap between the multiple plasmon resonances of the nanostars and the luminescence of the emitting polymers is one key for the substantial increase of the electroluminescence. The second key ingredient is the star-shaped morphology. Experiments quantifying the photoluminescence, electroluminescence, and the current–voltage characteristics reveal that the physical origins of the improved performance are twofold; first, a plasmon mediated increase of the radiative recombination of excitons, and second, an improved outcoupling of light otherwise trapped inside the OLEDs. The thin silica shell apparently minimizes exciton quenching via energy transfer and prevents the nanostars from short-cutting the active layer.

1. Introduction

Particle plasmons, resonant collective oscillations of the conduction electrons confined in nanoscale volumes, brought noble metal nanoparticles into the focus of extensive research in the last decades.[1,2] Localized plasmon resonances give rise to the unique optical properties of such nanoparticles, e.g., large scattering and absorption cross sections as well as strong field enhancements close to the particle surface. The strong electromagnetic fields in the vicinity of plasmonic nanostructures, so called hotspots, correlate with a large local density of optical states. Thus, the presence of plasmonic nanoparticles modifies light–matter interaction on the nanoscale. Accordingly, plasmonic nanoparticles have been used to enhance absorption,[3] to enhance or quench luminescence,[4,5] to spectrally reshape light emission,[6] to improve Raman scattering,[7–9] or to renormalize all Coulomb-mediated interactions, such as Förster resonance energy transfer.[10,11] Such light manipulation mechanisms are of particular interest for optoelectronic devices,[12] especially for organic light emitting diodes (OLEDs). Despite the enormous progress in improving the performance of OLEDs with new materials for the emitting as well as for the buffer layers,[13–16] conventional devices still suffer from a poor light outcoupling efficiency.[17–19] Although thin film morphologies were optimized[20,21] and new device architectures with additional light outcoupling structures were designed,[22–25] optimal light management in OLEDs still remains an open problem.[22] Recently, the incorporation of plasmonic nanoparticles in OLEDs was suggested as a promising strategy to enhance electroluminescence (EL).[26–36] The responsible mechanisms for the observed performance enhancement range from improved carrier injection[31,35] over improved light outcoupling[33] to triplet state quenching[26,34] and the acceleration of the radiative recombination of excitons.[29,32] For the latter, the most effective approach turns out to be the direct incorporation of nanoparticles with an appropriate dielectric coating in the active layer.[29,32] The dielectric coating allows to adjust the nominal distance between the excitons in the emitting layer and the plasmonic nanoparticles ensuring an optimal plasmon–exciton coupling.[29,32] A dielectric layer of around 10 nm efficiently reduces the exciton quenching by the metallic surface[29,37] and prevents charge transfer from the emissive layer to the nanoparticle.[29,38] Up to now, in most of the studies only spherical[27,29,30,32,35] or rod shaped nanoparticles[28,29] were incorporated in OLEDs, because even for these conventionally shaped nanoparticles, the incorporation into the active layer is a major challenge. Complex-shaped nanoparticles, such as nanostars, have been shown to outperform conventionally shaped nanoparticles in case of performance improvement of organic solar cells[39] or random lasers.[40] Nanostars are also a versatile tool for many applications where an optimal interaction between light and nanoscale objects is desirable, such as in biosensing[41–43] and for enhancing Raman signals.[44–46] However, there are no reports so far on their utilization in OLEDs.

B. Munkhbat, H. Pöhl, Prof. T. A. Klar, Dr. C. Hrelescu
Institute of Applied Physics
Johannes Kepler University Linz
4040 Linz, Austria
E-mail: calin.hrelescu@jku.at
P. Denk, Dr. M. C. Scharber
Linz Institute for Organic Solar Cells/Institute of Physical Chemistry
Johannes Kepler University Linz
4040 Linz, Austria

DOI: 10.1002/adom.201500702

Herein, we report the successful incorporation of silver-enhanced, star shaped gold nanoparticles, coated with a thin silica shell (AuAgNSts), in fully working OLEDs. An optimal overlap of the multiple plasmon resonances of the nanostars with the luminescence emission of two different polymers was achieved by controlling the size and sharpness of the nanostar tips and by silver-enhancement of the gold nanostars. Although gold nanostars provide strong and easily accessible hot-spots at their tips, additional silver coating improves their plasmonic properties by increasing the scattering cross-section.[47] The thickness of the silica shell is another essential parameter. The silica coating is thick enough to act as a spacer between the nanostars and the active layer to reduce luminescence quenching and as an insulator to prevent nanostar-induced shortcuts. However, it is thin enough to follow the nanostars' shape. This way, the nanostar tips, and the associated hot-spots, can protrude into the active layer, in contrast to previous reports on AuAgNSts, where the silica coating provided a thicker spherical shell.[47] For the two different polymers used as active layers, the OLEDs with incorporated non-aggregated AuAgNSts showed improved current–voltage characteristics as well as enhanced photo- and electroluminescence compared to the reference OLEDs without nanoparticles, whereas no significant changes in luminescence emission were observed for plasmonic OLEDs with silica-coated spherical gold nanoparticles or silica-coated gold nanostars without silver enhancement. Moreover, our experiments revealed that the angular distribution of the electroluminescence follows the angular distribution of the scattering of the nanostars. We find that the AuAgNSts can considerably enhance the electroluminescence of conventional OLEDs by acting as nanoantennas, thus accelerating the radiative recombination as well as improving the light outcoupling.

2. Results

Our studies are focused on the direct comparison of a polymer OLED architecture with nanoparticles incorporated in the active layer with a reference without nanoparticles. Among various light emitting materials, we chose two widely used polymers, namely Poly[2-methoxy-5-(2-ethylhexyloxy)-1,4-phenylene-vinylene]-end capped with Polysilsesquioxane (ADS200RE, often referred to as MEH-PPV) and Poly(9,9-dioctylfluorene-alt-benzothiadiazole), also known as F8BT. Both polymers, ADS200RE with luminescence emission in the orange spectral region (hereafter called orange emitter) and F8BT with luminescence emission in the green spectral region (hereafter called green emitter) exhibit high luminescence emission efficiencies and easy processability.[48,49]

The nanostars have to fulfill several crucial requirements in order to take advantage of their plasmonic properties and simultaneously avoid detrimental effects upon incorporation in the emissive layer. First, the nanostars have to spatially fit into the emissive layer, so that the incorporation will not cause major modifications of the device architecture or will not substantially increase the thickness of the emissive layer. Second, non-radiative exciton decay channels such as quenching due to the energy transfer or due to the charge carrier transfer to the metal should be minimized. Besides an optimal spectral overlap between the plasmon resonances of the nanostars and the luminescence emission of the active layer, the nanostars should not remarkably increase the light absorption, but in addition should improve the light outcoupling and the radiative exciton recombination. Furthermore, the nanostars should be chemically compatible with the solvents used for the device fabrication to avoid aggregation and ensure structural stability.

Considering the above-mentioned requirements, we designed two kinds of nanostars, gold nanostars (AuNSts) and silver-enhanced gold nanostars (AuAgNSts), both coated with a thin silica shell. Gold nanostars were synthesized in aqueous solution with an adapted seed-mediated method.[47] The detailed protocol of the synthesis can be found in the Experimental Section. The freshly synthesized gold nanostars were either coated only with a thin silica shell (AuNSts) or silver-enhanced and then coated with a thin silica shell (AuAgNSts). The silica shell allows mixing of the nanostars with organic solvents such as chlorobenzene without causing aggregation. In order to achieve a silica shell thickness of about 10 nm, the original recipe,[47] which provides substantially thicker shells, was modified by adjusting the concentrations of tetraethyl orthosilicate (TEOS) and ammonium hydroxide (NH_4OH) (see the Experimental Section for details).

Figure 1a,b shows transmission electron microscope (TEM) images of the synthesized AuNSts and AuAgNSts, respectively. The scale bar is 100 nm. Both types of nanostars have diameters in the range of 100 to 130 nm in order to fit into the emitting layer of 150 nm thickness. It is worth mentioning that the displayed nanostars stem from the same original batch of gold nanostars, half of which was branched off for silver-enhancement. The average silica shell thickness was of about 10 nm based on TEM image analysis of several nanoparticles. In both cases, the shell was uniformly and completely formed around the nanostars, maintaining their morphology. Due to the silica shell of about 10 nm, the excitonic sites of the emitting polymers are effectively outside the Förster radius.[50] However, the silica shell is thin enough to allow for photoluminescence enhancement.[5] In particular, since the thin silica shell follows the nanostars' shape, some excitonic sites can still be located in the hot-spots occurring at the tips of the nanostars.[51,52]

Due to their several sharp tips pointing in arbitrary directions, the AuNSts exhibit multiple plasmon resonances as well as high scattering cross-sections.[51,52] The spectral position of the plasmon resonances can be adjusted for an optimal spectral overlap with the emission of the light emitting polymers. In the green and orange spectral region this is achieved by silver-enhancement of the AuNSts. Figure 1c shows the ensemble averaged extinction spectra of the AuNSts and AuAgNSts dispersed in ethanol. Upon silver-enhancement, the plasmon resonances of the AuNSts progressively blueshift from around 900 nm down toward 530 nm. Besides the induced blueshifts of the plasmon resonances, the silver coating leads to a two-fold increase of the scattering efficiency without major changes in the nanostars' dimensions.[47] As can be seen from the TEM image in Figure 1b, the AuAgNSts still have several sharp tips protruding from the silver shell around their core. The observed blueshift can be attributed to the silver coating, leading to a mixed gold-silver dielectric function[53] as well as to a reduced aspect ratio of the nanostars' tips.[47] In particular, the plasmon

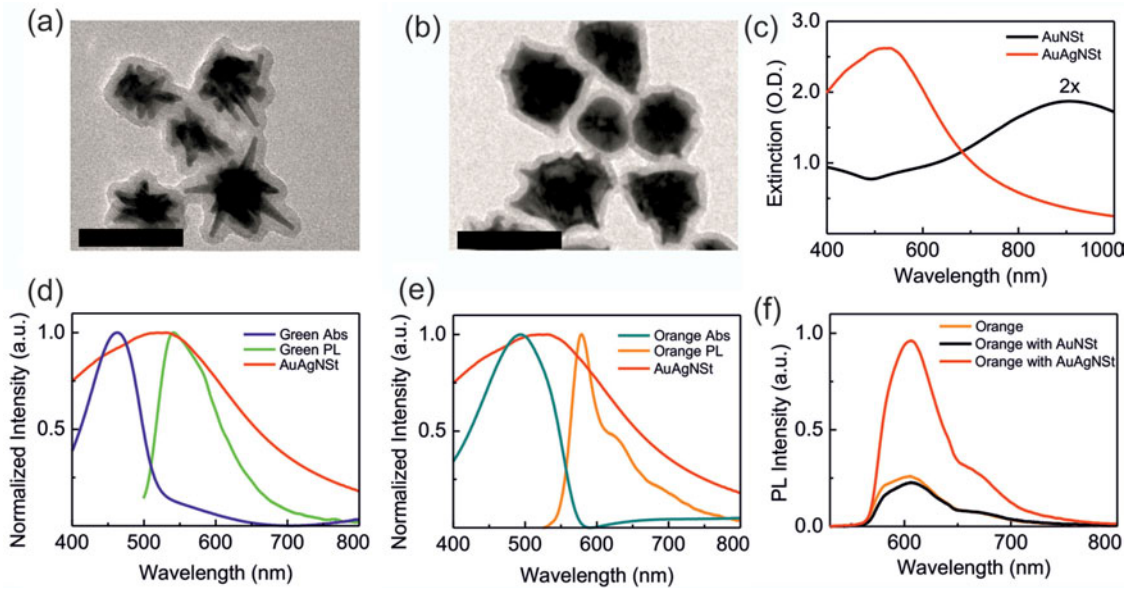

Figure 1. TEM images of a) AuNSts and b) AuAgNSts, the scale bar is 100 nm. c) Extinction spectra of AuNSts (black curve) and AuAgNSts (red curve) dispersed in ethanol. Normalized absorption (Abs) and photoluminescence spectra (PL) of d) green and e) orange polymers dissolved in chlorobenzene compared to the normalized AuAgNSts extinction spectrum (red curve). f) Comparison of the PL spectrum of a pure orange emitter dissolved in chlorobenzene (orange curve) with the PL spectra of solutions with same concentration of orange polymers containing either AuNSts (black curve) or AuAgNSts (red curve).

resonances of the synthesized AuAgNSts spectrally overlap with the absorption and photoluminescence (PL) emission of the orange emitting polymer (Figure 1d) and of the green emitting polymer (Figure 1e). Thus, the AuAgNSts fulfill all previously mentioned requirements for an optimized photon management in OLEDs.

Before incorporating the AuAgNSts and AuNSts in OLEDs, we investigated the influence of the two types of nanostars on the emission properties of the orange emitting polymer in solution. Three different solutions with the same concentration of the orange emitting polymer dissolved in chlorobenzene were prepared, hereafter called polymer solutions. Then, 200 µL of washed and concentrated AuNSts or AuAgNSts in chlorobenzene were added to 1 mL of the polymer solutions. Since the AuAgNSts were directly synthesized out of a part of the AuNSts, the concentrations are considered to be similar. The concentration of the AuAgNSts could even be slightly lower due to the additional washing steps required by the additional silver coating. Further, 200 µL of chlorobenzene without nanostars were added to 1 mL of the polymer solution to form the reference sample. Figure 1f shows the PL spectra of the three orange emitting polymer solutions with and without AuNSts and AuAgNSts. The polymer solutions were excited with a laser intensity of 138 mW cm^{-2} at 510 nm. The excitation wavelength lies within the maximal absorption of the polymer as well as the maximal extinction of the AuAgNSts solution. For the solution containing AuNSts (black spectrum in Figure 1f), a minor decrease in the photoluminescence compared to the reference (orange spectrum in Figure 1f) was observed. Compared to the reference solution and the solution containing AuNSts, the solution with AuAgNSts (red spectrum) shows a significant photoluminescence enhancement. Hence, we deduce that our silica shell thickness is sufficient to render quenching via energy or charge carrier transfer inefficient. Exhibiting the desired properties, the AuAgNSts were incorporated in an OLED architecture.

Figure 2a shows a schematic diagram of the fabrication procedure for the OLEDs (see the Experimental Section for details). In brief, the devices were fabricated on ITO-coated glass substrates as anode, covered with a spin-coated poly(3,4-ethylenedioxythiophene):polystyrene sulfonic acid (PEDOT:PSS) thin film (40 nm) as a hole injection layer (Step 1). After thermal annealing, nanostars in ethanol were spin-coated on top of the PEDOT:PSS, which allows to adjust their density and their subsequent incorporation in the active layer without major influences on the film morphology and thus the device architecture. An equivalent amount of pure ethanol as a reference was spin-coated on top of the PEDOT:PSS layer (Step 2) to ensure a fair comparison between the devices with and without nanoparticles, since the conductivity of PEDOT:PSS might be slightly changed upon addition of co-solvents such as ethanol.[54,55] The remaining fabrication steps are identical for all devices; a 150 nm thick emitting layer of the orange or green polymers was spin-coated on top of the PEDOT:PSS layer (Step 3) and the top electrode fingers were evaporated under high vacuum conditions (Step 4). The top electrodes consist of a 20 nm calcium (Ca) layer and a 100 nm silver (Ag) layer. Figure 2b,c shows the energy diagrams for the orange emitter and for the green emitter based OLED devices, respectively. Figure 2d,e shows photographs of typical samples of the orange and green OLEDs used in the experiments, respectively. Since the reference device and the device including nanoparticles were prepared at the same time and with identical fabrication steps, there are no noticeable differences in the film and device quality. The top electrodes were evaporated only on one half of the ITO substrates, forming

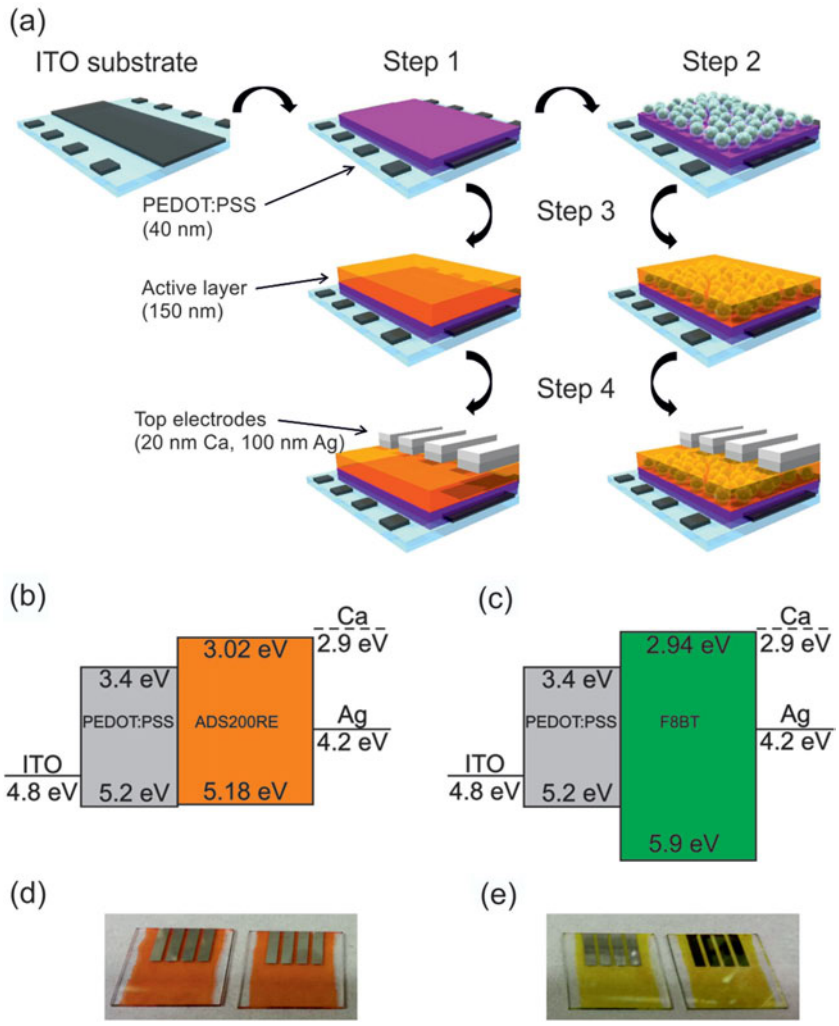

Figure 2. a) Schematic diagram illustrating the fabrication process of OLEDs with plasmonic nanoparticles. b,c) Energy diagrams and d,e) photographs of the orange emitting (left: without nanoparticles, right: with nanoparticles) and green emitting (left: without nanoparticles, right: with nanoparticles) OLED samples, respectively.

four similar OLEDs, while the other half of the sample enables the optical characterization.

Based on the respective emitting polymers, we shall conveniently denote the reference OLEDs as orange or green, while the devices with nanoparticles will hereafter be referred to as orange/AuAgNSt and green/AuAgNSt, respectively. The distribution and number density of AuAgNSts incorporated in the emissive layer were analyzed using true color micrographs of dark field white light scattering from the OLEDs. The true color micrographs were recorded with a charge-coupled device (CCD) camera mounted on a dark field microscope, while no voltage was applied to the OLEDs (see the Experimental Section for further details).

Figure 3a,b shows typical dark field optical micrographs of a reference and a plasmonic OLED, i.e., of orange and orange/AuAgNSt OLEDs (Figure 3a) and of a green and green/AuAgNSt OLEDs (Figure 3b). The images are true color images taken with a Nikon Digital Sight DS-5M red-green-blue (RGB) CCD camera. The emissive layers of the orange and green OLEDs are almost uniform and free of prominent scattering centers. The pale orange/green dots visible in their micrographs are polymer aggregates[56] already formed in the stock solution.[57] More examples are shown in Figure S1 in the Supporting Information. In the orange/AuAgNSt OLEDs (Figure 3a, right) and green/AuAgNSt OLEDs (Figure 3b, right), the nanostars are visible as bright orange and green dots, respectively. Except for a few aggregates, the nanostars are distributed homogeneously with an average interparticle distance of ≈2 µm. Additional examples of AuAgNSts distributions in several areas and from different orange/AuAgNSt OLEDs and green/AuAgNSt OLEDs are displayed in Figure S2 in the Supporting Information. In both plasmonic OLEDs, the number density was adjusted to be $\approx 6 \times 10^6$ nanostars in the active area (15 mm^2), which allows a direct comparison between different samples.

Figure 3c shows the current–voltage (*I–V*) and the luminance–voltage characteristics of the orange and of the orange/AuAgNSt OLEDs. Incorporating the AuAgNSts in the OLEDs leads to an increase in the voltage-dependent current-density for orange/AuAgNSt OLEDs (red curve in Figure 3c) compared to the reference OLEDs (orange). Furthermore, the orange/AuAgNSt OLEDs exhibit a substantially increased luminance (red dotted curve in Figure 3c) compared to the plain orange OLEDs (orange dotted), while the operating threshold voltages are almost identical. Figure 3d shows the current–voltage (*I–V*) and the luminance–voltage characteristics of the green and of the green/AuAgNSt OLEDs. At a given voltage, the green/AuAgNSt OLEDs show a bigger increase in the current-density and more enhanced luminance with respect to their reference compared to the orange/AuAgNSt OLEDs. Although the total number of nanostars in the orange/AuAgNSt OLEDs and green/AuAgNSt OLEDs is comparable, the incorporation of the AuAgNSts in the green OLEDs leads to a bigger improvement of the device performance.

The increase in the current-density can be attributed to a more efficient charge injection at the rougher interfaces between the different layers induced by the presence of AuAgNSts, in agreement with other reports.[58,59] To underline this, additional OLEDs with incorporated reference nanoparticles were prepared following the same processing steps as for the AuAgNSt OLEDs, but containing either silica coated AuNSts, plain silica spheres (125 nm in diameter), or silica-coated Au nanospheres (125 nm in diameter). The plasmon resonances of the silica-coated Au nanospheres also overlap spectrally with the luminescence emission of both polymers. The corresponding extinction spectrum is shown in Figure S3 of the Supporting Information. All additional OLEDs had a similar total number of the corresponding nanoparticles within the active area. The incorporation of plain

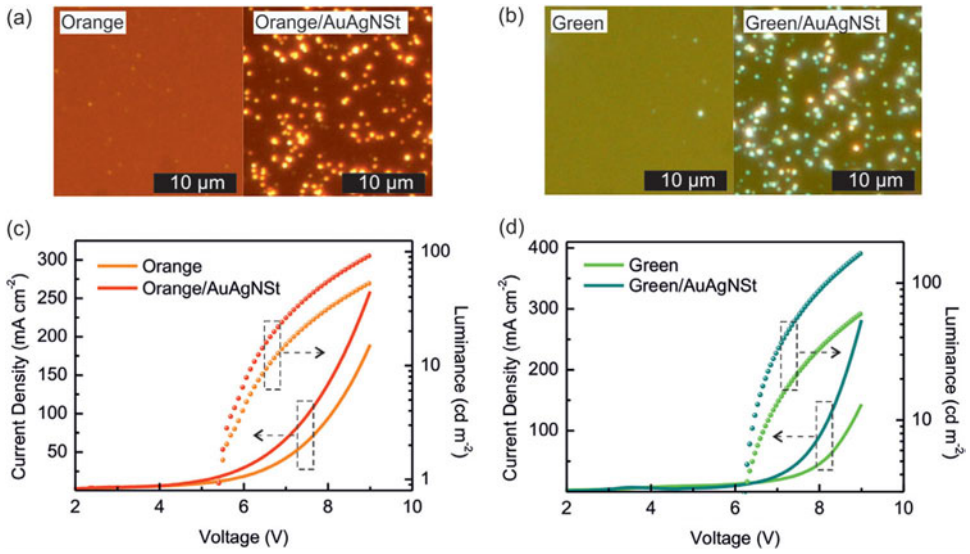

Figure 3. a,b) True color dark field micrographs of white light scattering from a reference and a plasmonic device featuring the orange emitter and the green emitter, respectively. For the dark field micrographs, no voltage was applied to the devices. c,d) Current–voltage characteristics (dotted lines) and luminance–voltage characteristics (solid lines) of orange and green OLEDs with and without AuAgNSts.

silica spheres and silica-coated Au nanospheres did not have any significant impact on the *I–V* characteristics of the OLEDs (Supporting Information, Figure S4a). In the case of the OLEDs with silica-coated AuNSts an akin increment in the current-density was observed as for the OLEDs with AuAgNSts (Supporting Information, Figure S4b). Since an improved charge carrier injection and a possible improved light outcoupling due to corrugation of the emissive layer might also lead to an increased luminance, it is premature, at this stage, to assign the observed enhanced luminance of the OLEDs containing AuAgNSts to a pure plasmonic origin.

In order to separate the contribution of a more efficient charge injection to the EL enhancement from plasmonic contributions to the EL enhancement, the EL spectra were taken for all OLEDs at the same driving current density. In **Figure 4**, the PL spectra of the OLEDs with and without

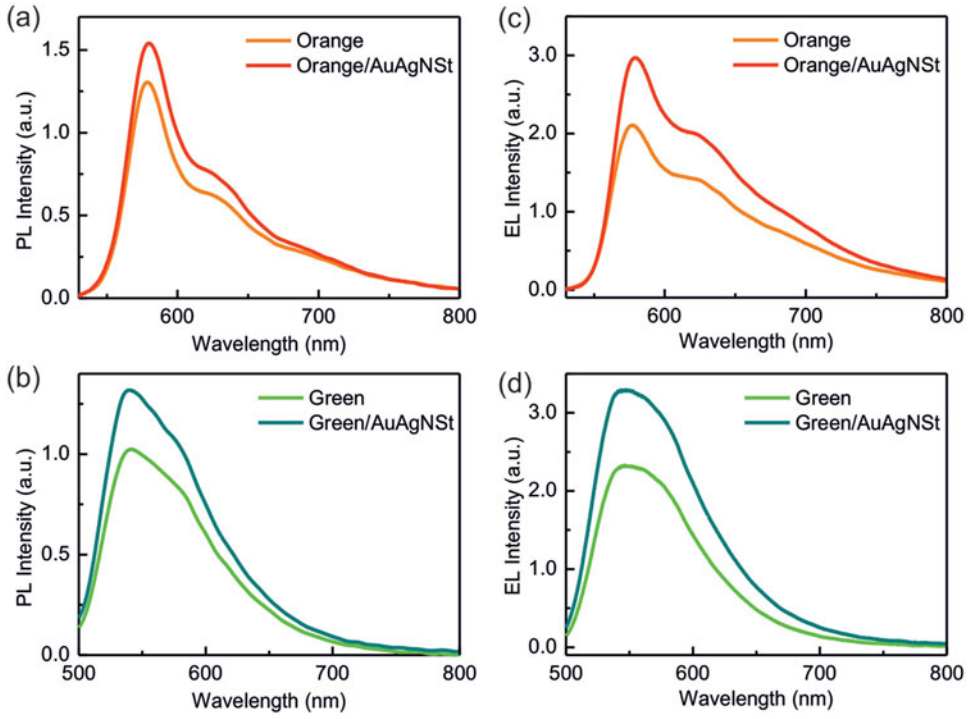

Figure 4. a,b) PL spectra of orange and green OLEDs with and without AuAgNSts. c,d) EL spectra of orange and green OLEDs with and without AuAgNSts, respectively, at a constant driving current density of 100 mA cm^{-2}.

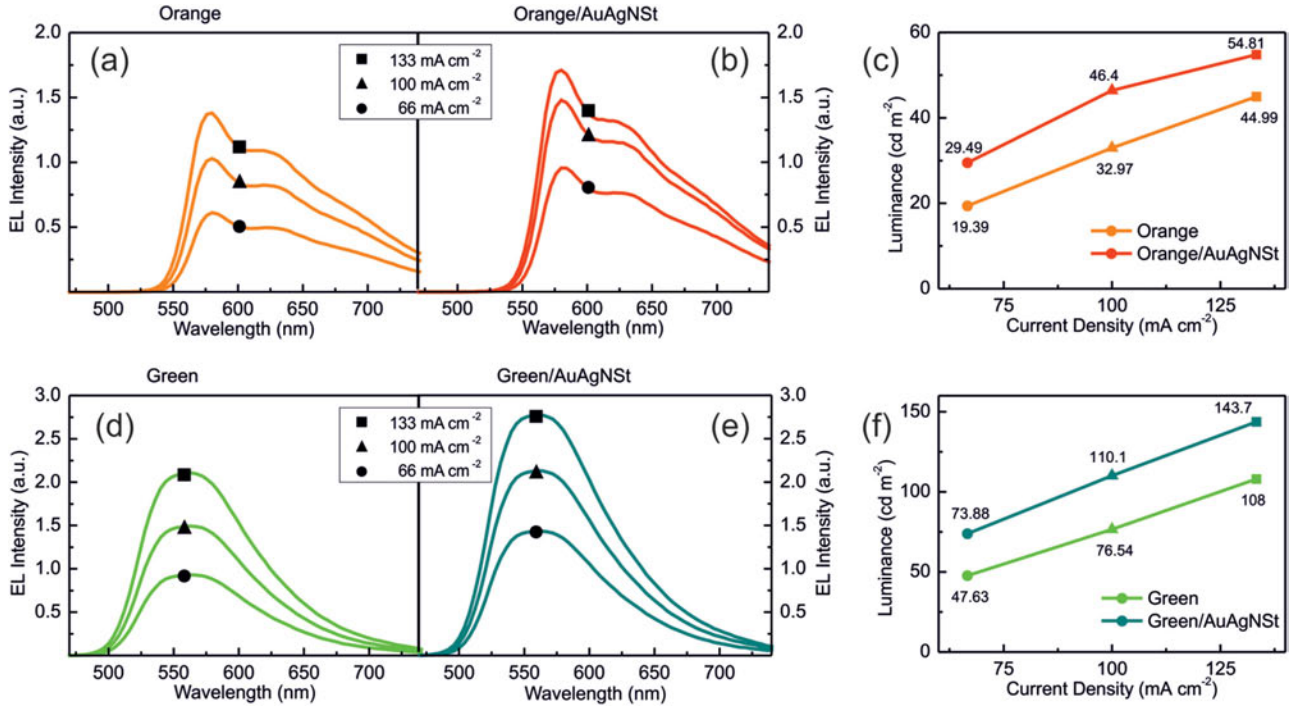

Figure 5. Injection current density dependent EL spectra and luminance of (a–c) orange and (d–f) green OLEDs with and without AuAgNSt, respectively.

AuAgNSts are compared to the corresponding EL spectra. Figure 4a shows PL spectra of the orange and the orange/AuAgNSt OLEDs upon laser excitation with 75 mW cm^{-2} at a wavelength of 500 nm. The green and green/AuAgNSt OLEDs were excited with 70 mW cm^{-2} at 470 nm. The corresponding PL spectra are displayed in Figure 4b. The excitation power in the PL experiments was chosen to be far below the nonlinear saturation regime. Both samples containing nanostars exhibit an enhanced PL compared to their references. For the orange/AuAgNSt OLEDs, a relative PL enhancement of 19% was measured in the wavelength range of 550 to 650 nm. Due to the better spectral overlap between the absorption/emission of the green polymer with the AuAgNSts plasmon resonances, the green/AuAgNSt OLEDs show 26% more PL intensity in the wavelength range of 520 to 620 nm than the reference green OLEDs (Figure 4b). We attribute the increase in PL primarily to the nanoantenna-induced excitation and emission enhancement by the AuAgNSt, see Section 3 below.

The EL intensities of the AuAgNSt OLEDs relative to the respective references are displayed in Figure 4c,d, respectively. Remarkably, one notices that for the OLEDs containing AuAgNSts, the EL is twice as much increased with respect to their references than the PL. The orange/AuAgNSt OLEDs exhibit a 36% EL improvement within the wavelength range of 550 to 650 nm, while for the green/AuAgNSt OLEDs, the EL is intensified by 44% with regard to the EL of the green reference OLEDs within the wavelength range of 520 to 620 nm. The observed EL intensification is reproducible for all 12 investigated AuAgNSt OLEDs, as shown in Figure S5 in the Supporting Information. Moreover, enhanced EL of the AuAgNSt OLEDs compared to the corresponding reference OLEDs is always significantly higher than the rather small EL intensity fluctuations due to device to device variation.

Using silica-coated Au nanospheres instead of AuAgNSts, no significant EL enhancement is observed for these plasmonic OLEDs (see the Supporting Information, Figure S6a), although the plasmon resonances spectrally overlap with the EL emission (Supporting Information, Figure S3). Also, the incorporation of plain silica spheres did not have significant influence on EL intensity with respect to the reference OLEDs. Further, in the case of AuNSts OLEDs, even a small decrease in the EL intensity compared to the reference was measured (see the Supporting Information, Figure S6b), consistent with the photoluminescence measurements in solution (Figure 1f). Since, for all OLEDs, the EL spectra were taken at the same driving current density of 100 mA cm^{-2}, the EL enhancement observed for AuAgNSt OLEDs with respect to the reference OLEDs (and all other OLEDs containing nanoparticles, including AuNSts) does not originate from a more efficient charge injection. In fact, the results strongly suggest that indeed the enhanced performance of AuAgNSt OLEDs has mainly a plasmonic origin.

In order to further quantify the EL enhancement, the dependence of the EL spectra and of the luminance on the injection current-density was measured. **Figure 5** shows the EL spectra and luminance of orange and green OLEDs with and without AuAgNSts for various injection current densities ranging from 66 to 133 mA cm^{-2}. Compared to the reference orange OLEDs in Figure 5a, the EL of the orange/AuAgNSt OLEDs in Figure 5b is enhanced for all injection current densities, but with increasing injection current densities, the EL intensity starts to reach saturation.

It turns out that for lower injection current densities, the relative luminance enhancement is about 50% compared to the reference OLEDs. Also, for the green/AuAgNSt OLEDs, a maximum luminance enhancement of about 50% with respect

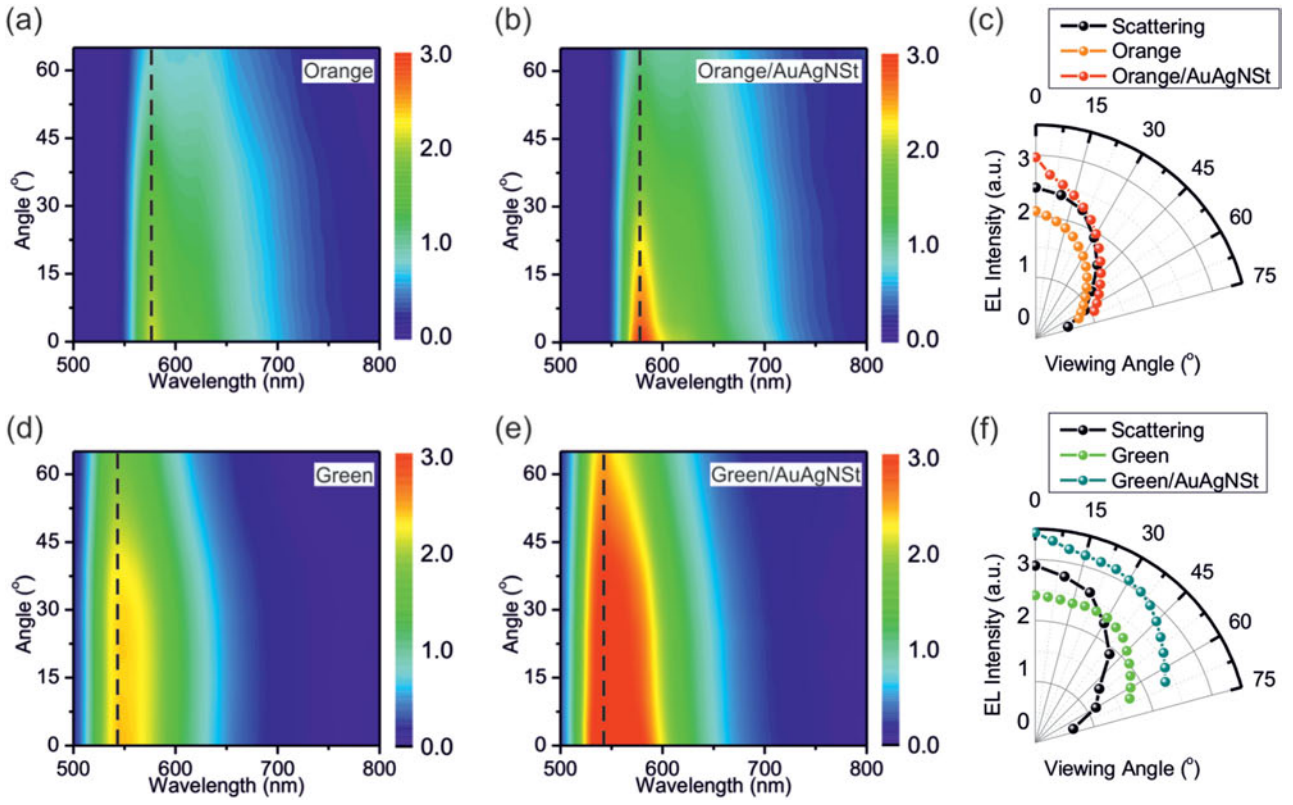

Figure 6. Angle-resolved EL spectra of a,b) the orange and d,e) the green OLEDs with and without AuAgNSts, respectively. c,f) EL intensities of orange and green OLEDs with and without AuAgNSts and the scattering of AuAgNSts on PEDOT:PSS as a function of the viewing angle, evaluated at the fixed wavelength of the maximal EL emission intensity, marked with dashed lines in the 2D false color plots of angle-resolved EL spectra.

to the reference is achieved for low injection current densities. In contrast to the orange/AuAgNSt OLEDs, the green/AuAgNSt OLEDs don't exhibit a saturation behavior of the EL intensity with increasing injection current densities and hence not for the luminance, too.

In order to further investigate the influence of the AuAgNSts on the EL emission, we recorded the EL emission spectra for several emission angles with respect to the surface normal. **Figure 6**a,b shows the angle-resolved EL emission spectra as 2D false color plots for the orange and orange/AuAgNSt OLEDs, respectively. The angle-resolved EL spectrum of the orange/AuAgNSt OLEDs reveals that a significantly enhanced EL can be observed mostly in the forward direction, i.e. for angles smaller than 30° with respect to the surface normal. For larger angles, the EL intensity becomes comparable to the intensity of the reference OLEDs. The angular distributions of the EL emission intensity at 580 nm are displayed for the orange and the orange/AuAgNSt OLEDs as polar diagrams in Figure 6c. The plain orange OLEDs exhibit a purely Lambertian EL emission behavior, while the EL emission of the orange/AuAgNSt OLEDs deviates from the Lambertian emission behavior for angles smaller than 30°.

The corresponding angle-resolved EL emission spectra of the green emitting OLEDs and the green/AuAgNSt OLEDs in Figure 6d,e reveal that neither of the two OLEDs shows a Lambertian EL emission characteristic. Moreover, for each observation angle larger than 15°, the EL intensity from the green/AuAgNSt OLEDs is equally increased compared to the EL intensity of the green reference OLEDs, as can be seen in the polar diagram of the angular distribution of the EL emission intensities at 540 nm in Figure 6f. For the forward direction, i.e. observation angles smaller than 15° with respect to the surface normal, the green/AuAgNSt OLEDs show a different angular distribution of EL emission intensity compared to the reference OLEDs. This characteristic is similar to the angular EL emission characteristics of the orange/AuAgNSt OLEDs, but the deviation from the reference OLEDs emission characteristic is not as pronounced.

The scattering of AuAgNSts on PEDOT:PSS (black curves in Figure 6c,f) shows strong similarities in angular dispersion to the observed angular EL emission characteristics of the plasmonic OLEDs. The 2D false color plots of the angle resolved scattering spectra can be found in Figure S7 in the Supporting Information. In fact, the angular EL dispersion characteristics of the plasmonic OLEDs can be explained as a convolution of the EL emission of the corresponding plain OLEDs and the scattering of the AuAgNSts. (Figure 6c,f and Figure S8 in the Supporting Information).

3. Discussion

There are several contributions which might lead to a luminescence modification, namely (1a) an excitation enhancement in PL, (1b) an improved charge carrier injection in EL, (2) an

increase of nonradiative decay channels caused by nanoparticles (quenching via Förster energy transfer), (3) a plasmon-mediated decrease (3a) or an increase (3b) of the radiative rate, and (4) an enhanced scattering out of OLEDs. We discuss them now point by point:

(1a) Excitation Enhancement: The plasmon resonances of the AuAgNSts spectrally overlap with the absorption of the polymers. Upon optical excitation with a wavelength corresponding to the maximal absorption of the respective polymer, the AuAgNSts provide strong hot-spots located at their tips, leading to a substantial excitation enhancement of the polymers, which contributes to the observed, considerably increased PL of polymer solutions (Figure 1f) and to the increased PL of OLEDs containing AuAgNSts (Figure 4a,b) compared to the respective references.

(1b) Improved Charge Carrier Injection: Similar to the excitation enhancement in the PL, an improved charge carrier injection may lead to an increased generation of excitons. The incorporation of nanoparticles induces a corrugation of the emissive layer in the plasmonic OLEDs. The altered current–voltage characteristics of the OLEDs containing AuAgNSts (Figure 3c,d) and AuNSts (Figure S4 in the Supporting Information) reveal that the charge injection could be more efficient in these plasmonic OLEDs due to the nanoscopically roughened surface (Figure S9 in the Supporting Information). However, in the EL experiments, a constant driving current density was used for all the OLEDs (reference and plasmonic) in order to exclude EL modifications due to differences in the charge injection efficiencies. Hence, the increased EL in Figure 4c,d cannot be explained by increased charge carrier injection (see also Figure S10 in the Supporting Information).

(2) Quenching via Förster Energy Transfer: In order to minimize exciton quenching (energy transfer to the nanoparticles), all used nanoparticles (spheres, AuAgNSts and AuNSts) were coated with a thin silica shell, so that most of the excitonic sites are effectively located outside the Förster radius. Since for all samples containing AuAgNSts (solutions and OLEDs) a substantially enhanced luminescence emission was measured, quenching by the AuAgNSts can only play a minor role. Moreover, as no significant changes in EL intensities for OLEDs containing silica-coated Au nanospheres or AuNSts compared to the reference were observed (Figure S6 in the Supporting Information), we can conclude that quenching is not dominant in all investigated plasmonic OLEDs.

(3) Plasmon Mediated Changes of the Radiative Rate: In the presence of plasmonic nanoparticles, the in-phase or out-of-phase coupling of singlet excitons with dipolar plasmonic modes can decrease (3a) or increase (3b) the overall radiative rate, respectively.[60] In our experiments, either considerably enhanced EL of AuAgNSt OLEDs (Figures 4 and 5, as well as Figure S5 in the Supporting Information) or no apparent differences between the EL of the plain reference OLEDs and the EL of plasmonic OLEDs with incorporated silica-coated spherical gold nanoparticles or silica-coated gold nanostars were observed (Figure S6 in the Supporting Information). Hence, a meaningfully decreased radiative rate (case 3a) can be excluded. Furthermore, in all investigated plasmonic OLEDs, a plasmon mediated increase of the radiative rate (case 3b) is more than plausible. The nearly unaffected EL intensity of the plasmonic OLEDs with silica-coated Au nanospheres and of AuNSts with respect to the reference OLEDs can be attributed to increased radiative rates of excitons which counterbalance the nonradiative rates, especially the residual quenching in the vicinity of silica-coated Au nanospheres and of AuNSts, which takes place despite the silica shell. In the case of the AuAgNSts/OLEDs, the considerably enhanced PL and EL indicate a substantially increased radiative rate that outweighs all the non radiative rates, particularly the energy transfer rate to the nanoparticles. Compared to other nanoparticles used in this study, the AuAgNSts provide two advantages for a plasmon mediated increase of the radiative rate: first, their plasmon resonances spectrally overlap with the luminescence of the emitting polymers. This also holds true for the silica-coated Au nanospheres. However, in this case, no EL enhancement is observed. The second advantage must be the asymmetric shape of AuAgNSts. Since the individual AuAgNSts have several randomly oriented tips, it is highly probable that at least one of these tips points in an advantageous direction for in-phase coupling of a tip-plasmon to a nearby dipolar moment of singlet excitons in the emissive layer. Due to the spectral overlap, such in-phase exciton–plasmon coupling will increase the radiative rate of nearby singlet excitons substantially.

(4) Enhanced Scattering out of OLEDs: Our experiments revealed that the angular EL dispersion characteristics of the OLEDs containing AuAgNSts can be understood as the convolution of the scattering of the AuAgNSts and the EL emission of the corresponding plain OLEDs (Figure 6c,f and Figure S8 in the Supporting Information). Consequently, the AuAgNSts can improve the light outcoupling by enhancing the scattering out of OLEDs. Further, the plasmon modes of the AuAgNSts could couple to different optical modes in the OLEDs, such as propagating surface plasmons at the silver electrode/emissive layer interface. Also, in this case, the asymmetric shapes of AuAgNSts offer higher probabilities that at least some of the several tips have advantageous orientations so that different optical modes can couple to the corresponding plasmon resonances. Subsequently, photons with the frequency of the coupled resonance could be scattered out of the OLEDs, so that light otherwise trapped in different optical modes in the OLEDs can be recovered. Therefore, the scattering of the AuAgNSts, which spectrally matches the EL emission and the improved light-outcoupling mechanisms, induced by the complex morphology of the AuAgNSts, can also contribute to the observed improvements in light emission.

4. Conclusions

We have shown that the incorporation of silver-enhanced gold nanostars coated with a thin silica shell in fully working OLEDs provides remarkable improvements in device performance. Compared to conventional OLEDs without nanoparticles, the OLEDs with incorporated AuAgNSts showed increased current-densities as well as substantially enhanced photo- and electroluminescence. In particular, for low injection currents, the electroluminescence of conventional OLEDs can be enhanced up to 50% with AuAgNSts. The observed luminescence enhancements have predominantly plasmonic origins, namely an increased radiative rate of singlet excitons in the vicinity of

the AuAgNSts and improved light outcoupling. We find that the relevant parameters for luminescence enhancement are the anisotropic shape of the nanostars and the spectral overlap between the plasmon resonances and the luminescence of the emitting polymers. Compared to the plasmonic contributions, the improved charge injection plays apparently a minor role for the EL enhancement.

Furthermore, the simultaneous compatibility of the AuAgNSts with organic and water-based solvents and their plasmonic properties make them one of the most promising candidates for effective photon-management in organic and inorganic optoelectronic devices. The AuAgNSts may bring substantial advantages in biosensing and analytics applications, where an optimal balance between light emission enhancement and quenching, high scattering cross-sections and easily accessible hot-spots provided by AuAgNSts are also highly desirable.

5. Experimental Section

Materials: Silver nitrate ($AgNO_3$, 99.9999%), Gold(III) chloride trihydrate ($HAuCl_4{\cdot}3H_20$), L-ascorbic acid (AA), tetraethyl TEOS, trisodium citrate dihydrate, 1 N hydrochloric acid solution (HCl), hexadecyltrimethylammonium bromide (CTAB), *O*-[2-(3-Mercaptopropionylamino)ethyl]-*O*-methylpoly(ethylene glycol) (mPEG-SH, MW 5K), ammonium hydroxide (NH_4OH, 30%) were purchased from Sigma-Aldrich at the highest purity grade available. Commercial PEDOT:PSS in water (Clevios PH), Poly[2-methoxy-5-(2-ethylhexyloxy)-1,4-phenylene-vinylene]-end capped with Polysilsesquioxane (ADS200RE, purchased from American Dye Source), Poly[(9,9-dioctylfluorenyl-2,7-diyl)-alt-(benzo[2,1,3]thiadiazol-4,7-diyl)] (F8BT, purchased from Lumtec) were used without further purification. Carbon-coated copper TEM grids were purchased from Plano GmbH. Ethanol absolute (99.9%) was purchased from Fisher Chemical. All glassware and stir bars were thoroughly cleaned with *aqua regia* and dried prior to use. Ultrapure distilled water (Millipore, 18 MΩ cm) was used in all preparations.

Synthesis of Silver-Enhanced Gold Nanostars: Silver-coated gold nanostars (AuAgNSts) were synthesized according to the literature.[47] In brief, using the Turkevich method,[61] a 12 nm gold seed solution was prepared by adding 15 mL of 1% trisodium citrate to 100 mL of a boiling solution of 1×10^{-3} M $HAuCl_4$. The solution was kept boiling for an additional 15 min, cooled down to room temperature in an ice bath, filtered through a 0.2 µm polyethersulfone membrane, and stored at 4 °C until use. For the gold nanostars (AuNSts) 100 µL of the aged seed were added to 10 mL of an aqueous growth solution of 0.25×10^{-3} M gold chloride ($HAuCl_4$). The pH was adjusted by adding 10 µL of 1 N HCl. Then, 100 µL of 3×10^{-3} M silver nitrate ($AgNO_3$) and 50 µL of 0.1 M ascorbic acid were simultaneously added to the growth solution under vigorous stirring. Immediately after the synthesis, the nanostars were functionalized with CTAB, i.e., 100 µL of 0.1 M CTAB was added to the AuNSts solution and left stirring for 5 min. The nanostars were washed by centrifugation (2000 rcf for 20 min), and redispersed in a 10 mL of 1×10^{-3} M aqueous CTAB solution. For silver enhancement, 30 µL of 0.1 M $AgNO_3$ and an equivalent volume of 0.1 M AA were added to the AuNSts solution under vigorous stirring. The reduction of silver ions by AA was initiated by adding 20 µL of 30% NH_4OH solution, at which point the color of the solution darkens. After 15 min, the AuAgNSts were purified by centrifugation at 2000 rcf for 10 min, discarding the supernatant, and redispersed in 10 mL distilled water.

Silica Encapsulation of AuAgNSts: The freshly synthesized AuAgNSts (10 mL) were capped with 5×10^{-6} M final concentration mPEG-SH under gentle stirring for 1 h. The PEGylated AuAgNSts were washed once by centrifugation (2500 rcf for 10 min) and redispersed in a mixed solution of EtOH (9 mL) and water (2 mL). Under gentle stirring, silica coating was initiated by adding 100 µL of NH_4OH followed by 30 µL of 10% TEOS in EtOH. The reaction was allowed to proceed for 12 h, at which point the AuAgNSts were washed three times by centrifugation at 3000 rcf for 5 min and redispersed in EtOH or chlorobenzene.

Nanoparticle Characterization Methods: The extinction spectra of the silica encapsulated AuAgNSts and silica encapsulated AuNSts were measured by a Varian Cary 500 Scan UV–Vis–NIR spectrophotometer. For the morphology characterization with a TEM, the nanoparticle solution was drop casted on carbon-coated copper TEM grids, let dry and analyzed using a JEOL JEM-2010 TEM.

Device Fabrication: The devices were fabricated on patterned ITO-coated glass substrates with a sheet resistance of 15 Ω sq^{-1}. The ITO-coated glass substrates were cleaned with acetone and isopropanol, respectively, to remove impurities. Then, PEDOT:PSS was spin-coated onto ITO surface to form a 40 nm thin layer. Subsequently, the substrates were annealed on a hot plate at 150 °C for 20 min. Due to the insolubility of PEDOT:PSS in ethanol, the silica-coated AuAgNSts in ethanol solution can be directly spin-coated on top of the PEDOT:PSS layer and annealed at 80 °C for 5 min to remove excess ethanol. For orange and green OLEDs, ADS200RE as orange emitting polymer and F8BT as green emitting polymer were dissolved in chlorobenzene and stirred at 70 °C for 12 h, respectively. The solutions were spin-coated on top of the PEDOT:PSS layer to produce 150 nm thick films and were afterward annealed on a hot plate at 80 °C for 10 min. The top electrode fingers (20 nm Ca, 100 nm Ag) were evaporated under high vacuum conditions (5×10^{-6} mbar) to create a device with an active area of 15 mm^2 defined by a shadow mask. A device without AuAgNSts was used as a reference.

Emissive Layer Characterization: The distributions of the different nanoparticles within OLEDs were investigated using a Nikon L-UEPI dark field microscope with 100×/0.90 NA objective lens and a 100 W halogen lamp as excitation source. For further analysis, white light scattering dark-field images were recorded with the color CCD-CAMERA (Nikon Digital Sight DS-5M). The number density of nanoparticles on the measured samples was determined with ImageJ[62,63] by using a 2D Gaussian fitting routine provided by the ImageJ SMLM GDSC plugin.[64] Dark-field images of reference samples and samples with nanoparticles were converted into grayscale images by simply splitting their RGB channels. Then, a small area of the sample (typically 20 by 20 µm) was evaluated manually. The parameters of a 2D Gaussian fitting routine were subsequently adjusted to match these manual results. Finally, this fitting routine was applied to a substantially larger area of the image (typically 200 × 200 µm). The number of counts was then divided by the sampling area to retrieve the number density. It has to be noted that this counting procedure can be performed both on bare particles on PEDOT:PSS and after full coverage of particles with the active layer. In the latter case, the appropriate selection of a specific RGB channel allows sufficient contrast between polymer background (mainly fluorescence) and the scattering of the nanoparticles.

OLEDs Characterization: The performance of the fabricated OLEDs was measured using an Agilent B1500 parameter analyzer with two source meter units, one driving the OLEDs and one measuring the resulting photocurrent in a silicon diode. The angle-resolved EL spectra were recorded using a spectrometer (Thorlabs CCS175) by applying constant current density with source-measure unit (Keithley 2401). The optical axis for detection is fixed, while the OLED (substrate surface normal) was rotating with respect to the detection optical axis from 0° to 70°. Current density-dependent EL measurements were performed using a Photo Research Spectrascan PR-655 and a Keithley SMU 2401. PL spectra were measured on a separate self-built setup equipped with a spectrometer (Thorlabs CCS175).

Supporting Information

Supporting Information is available from the Wiley Online Library or from the author.

Acknowledgements

The authors gratefully acknowledge valuable discussions with Prof. Sariciftci, and would like to cordially thank Heidi Piglmayer-Brezina

and Wolfgang Grafeneder for taking the SEM and TEM images. B.M. acknowledges the financial support by the Erasmus Mundus Mobility Project GATE. Further, the authors acknowledge financial support by the European Research Council (ERC Starting Grant No. 257158 "Active NP"), by the Austrian Science Foundation (FWF) within the Wittgenstein Prize Scheme for Prof. Sariciftci (FWF [Z 222-N19] SolareEnergieumwandlung), and by the Austrian Klima-und Energiefonds (SolarTrap, Grant No. 843929).

Received: November 26, 2015
Revised: February 9, 2016
Published online: March 14, 2016

[1] U. Kreibig, M. Vollmer, *Optical Properties of Metal Clusters*, Springer, Berlin, Germany **1995**.
[2] S. A. Maier, *Plasmonics: Fundamentals and Applications*, Springer, New York **2007**.
[3] D. M. Schaadt, B. Feng, E. T. Yu, *Appl. Phys. Lett.* **2005**, *86*, 063106.
[4] E. Dulkeith, A. C. Morteani, T. Niedereichholz, T. A. Klar, J. Feldmann, S. A. Levi, F. C. J. M. van Veggel, D. N. Reinhoudt, M. Möller, D. I. Gittins, *Phys. Rev. Lett.* **2002**, *89*, 203002.
[5] P. Anger, P. Bharadwaj, L. Novotny, *Phys. Rev. Lett.* **2006**, *96*, 113002.
[6] M. Ringler, A. Schwemer, M. Wunderlich, A. Nichtl, K. Kürzinger, T. A. Klar, J. Feldmann, *Phys. Rev. Lett.* **2008**, *100*, 203002.
[7] S. Nie, S. R. Emory, *Science* **1997**, *275*, 1102.
[8] K. Kneipp, Y. Wang, H. Kneipp, L. T. Perelman, I. Itzkan, R. R. Dasari, M. S. Feld, *Phys. Rev. Lett.* **1997**, *78*, 1667.
[9] M. Ringler, T. A. Klar, A. Schwemer, A. S. Susha, J. Stehr, G. Raschke, S. Funk, M. Borowski, A. Nichtl, K. Kürzinger, R. T. Phillips, J. Feldmann, *Nano Lett.* **2007**, *7*, 2753.
[10] M. Durach, A. Rusina, V. I. Klimov, M. I. Stockman, *New J. Phys.* **2008**, *10*, 105011.
[11] V. Faessler, C. Hrelescu, A. A. Lutich, L. Osinkina, S. Mayilo, F. Jaeckel, J. Feldmann, *Chem. Phys. Lett.* **2011**, *508*, 67.
[12] H. A. Atwater, A. Polman, *Nat. Mater.* **2010**, *9*, 205.
[13] H. Sasabe, J. Kido, *Chem. Mater.* **2011**, *23*, 621.
[14] H. Lin, J.-S. Yu, W. Zhang, *Optoelectron. Lett.* **2012**, *8*, 197.
[15] S. I. Yoo, J. A. Yoon, N. H. Kim, J. W. Kim, J. S. Kang, C.-B. Moon, W. Y. Kim, *J. Lumin.* **2015**, *160*, 346.
[16] C.-H. Shih, P. Rajamalli, C.-A. Wu, W.-T. Hsieh, C.-H. Cheng, *ACS Appl. Mater. Interfaces* **2015**, *7*, 10466.
[17] P. A. Hobson, J. A. E. Wasey, I. Sage, W. L. Barnes, *IEEE J. Sel. Top. Quantum Electron.* **2002**, *8*, 378.
[18] L. H. Smith, J. A. E. Wasey, I. D. W. Samuel, W. L. Barnes, *Adv. Funct. Mater.* **2005**, *15*, 1839.
[19] S. Nowy, B. C. Krummacher, J. Frischeisen, N. A. Reinke, W. Brütting, *J. Appl. Phys.* **2008**, *104*, 123109.
[20] Y. Shi, J. Liu, Y. Yang, *J. Appl. Phys.* **2000**, *87*, 4254.
[21] M. Rippa, R. Capasso, L. Petti, G. Nenna, A. D. G. D. Mauro, M. G. Maglione, C. Minarini, *J. Mater. Chem. C* **2014**, *3*, 147.
[22] K. Saxena, V. K. Jain, D. S. Mehta, *Opt. Mater.* **2009**, *32*, 221.
[23] W. Ding, Y. Wang, H. Chen, S. Y. Chou, *Adv. Funct. Mater.* **2014**, *24*, 6329.
[24] Q.-D. Ou, L. Zhou, Y.-Q. Li, J.-D. Chen, C. Li, S. Shen, J.-X. Tang, *Adv. Opt. Mater.* **2015**, *3*, 87.
[25] B. Jiao, Y. Yu, Y. Dai, X. Hou, Z. Wu, *Opt. Express* **2015**, *23*, 4055.
[26] J. H. Park, Y. T. Lim, O. O. Park, J. K. Kim, J.-W. Yu, Y. C. Kim, *Chem. Mater.* **2004**, *16*, 688.
[27] A. Fujiki, T. Uemura, N. Zettsu, M. Akai-Kasaya, A. Saito, Y. Kuwahara, *Appl. Phys. Lett.* **2010**, *96*, 043307.
[28] T. Tanaka, Y. Totoki, A. Fujiki, N. Zettsu, Y. Miyake, M. Akai-Kasaya, A. Saito, T. Ogawa, Y. Kuwahara, *Appl. Phys. Express* **2011**, *4*, 032105.
[29] F. Liu, J.-M. Nunzi, *Appl. Phys. Lett.* **2011**, *99*, 123302.
[30] Y. Xiao, J. P. Yang, P. P. Cheng, J. J. Zhu, Z. Q. Xu, Y. H. Deng, S. T. Lee, Y. Q. Li, J. X. Tang, *Appl. Phys. Lett.* **2012**, *100*, 013308.
[31] F. Liu, J.-M. Nunzi, *Org. Electron.* **2012**, *13*, 1623.
[32] T. Kim, H. Kang, S. Jeong, D. J. Kang, C. Lee, C.-H. Lee, M.-K. Seo, J.-Y. Lee, B. J. Kim, *ACS Appl. Mater. Interfaces* **2014**, *6*, 16956.
[33] Y. Gu, D.-D. Zhang, Q.-D. Ou, Y.-H. Deng, J.-J. Zhu, L. Cheng, Z. Liu, S.-T. Lee, Y.-Q. Li, J.-X. Tang, *J. Mater. Chem. C* **2013**, *1*, 4319.
[34] K. Xu, Y. Li, W. Zhang, L. Zhang, W. Xie, *Curr. Appl. Phys.* **2014**, *14*, 53.
[35] H. Sung, J. Lee, K. Han, J.-K. Lee, J. Sung, D. Kim, M. Choi, C. Kim, *Org. Electron.* **2014**, *15*, 491.
[36] P. Mucur, E. Tekin, S. E. San, Ö. Duygulu, H. Ü. Öztürk, G. Utkan, A. A. Denizci, *Opt. Mater.* **2015**, *47*, 297.
[37] N. S. Abadeer, M. R. Brennan, W. L. Wilson, C. J. Murphy, *ACS Nano* **2014**, *8*, 8392.
[38] M. Salvador, B. A. MacLeod, A. Hess, A. P. Kulkarni, K. Munechika, J. I. L. Chen, D. S. Ginger, *ACS Nano* **2012**, *6*, 10024.
[39] D. Kozanoglu, D. H. Apaydin, A. Cirpan, E. N. Esenturk, *Org. Electron.* **2013**, *14*, 1720.
[40] J. Ziegler, M. Djiango, C. Vidal, C. Hrelescu, T. A. Klar, *Opt. Express* **2015**, *23*, 15152.
[41] S. K. Dondapati, T. K. Sau, C. Hrelescu, T. A. Klar, F. D. Stefani, J. Feldmann, *ACS Nano* **2010**, *4*, 6318.
[42] J. R. G. Navarro, A. Liotta, A.-C. Faure, F. Lerouge, F. Chaput, G. Micouin, P. L. Baldeck, S. Parola, *Langmuir* **2013**, *29*, 10915.
[43] D. Jana, C. Matti, J. He, L. Sagle, *Anal. Chem.* **2015**, *87*, 3964.
[44] E. S. Allgeyer, A. Pongan, M. Browne, M. D. Mason, *Nano Lett.* **2009**, *9*, 3816.
[45] C. Hrelescu, T. K. Sau, A. L. Rogach, F. Jackel, J. Feldmann, *Appl. Phys. Lett.* **2009**, *94*, 153113.
[46] A. M. Fales, H. Yuan, T. Vo-Dinh, *Langmuir* **2011**, *27*, 12186.
[47] A. M. Fales, H. Yuan, T. Vo-Dinh, *J. Phys. Chem. C* **2014**, *118*, 3708.
[48] J. H. Burroughes, D. D. C. Bradley, A. R. Brown, R. N. Marks, K. Mackay, R. H. Friend, P. L. Burns, A. B. Holmes, *Nature* **1990**, *347*, 539.
[49] C. R. McNeill, N. C. Greenham, *Adv. Mater.* **2009**, *21*, 3840.
[50] T. Förster, *Ann. Phys.* **1948**, *437*, 55.
[51] C. L. Nehl, H. Liao, J. H. Hafner, *Nano Lett.* **2006**, *6*, 683.
[52] C. Hrelescu, T. K. Sau, A. L. Rogach, F. Jaeckel, G. Laurent, L. Douillard, F. Charra, *Nano Lett.* **2011**, *11*, 402.
[53] S. Link, Z. L. Wang, M. A. El-Sayed, *J. Phys. Chem. B* **1999**, *103*, 3529.
[54] Y. Xia, J. Ouyang, *J. Mater. Chem.* **2011**, *21*, 4927.
[55] D. Alemu, H.-Y. Wei, K.-C. Ho, C.-W. Chu, *Energy Environ. Sci.* **2012**, *5*, 9662.
[56] J. Vogelsang, T. Adachi, J. Brazard, D. A. Vanden Bout, P. F. Barbara, *Nat. Mater.* **2011**,*10*, 942.
[57] T.-Q. Nguyen, V. Doan, B. J. Schwartz, *J. Chem. Phys.* **1999**, *110*, 4068.
[58] S. A. Carter, J. C. Scott, P. J. Brock, *Appl. Phys. Lett.* **1997**, *71*, 1145.
[59] Y. Bai, Y. Fan, Q. Lu, X. Wang, M. Chu, X. Liu, *Appl. Phys. Express* **2015**, *8*, 022102.
[60] T. A. Klar, J. Feldmann, in *Complex-Shaped Metallic Nanoparticles* (Eds: T. K. Sau, A. L. Rogach), Wiley-VCH, Weinheim, Germany **2012**, pp. 395–427 .
[61] J. Turkevich, P. C. Stevenson, J. Hillier, *Discuss. Faraday Soc.* **1951**, *11*, 55.
[62] M. D. Abramoff, P. J. Magalhães, S. J. Ram, *Biophotonics Int.* **2004**, *11*, 36.
[63] National Institutes of Health, ImageJ, http://imagej.nih.gov/ij/index.html (accessed: November 2015).
[64] A. Herbert, GDSC-SMLM - GDSC Single Molecule Light Microscopy ImageJ Plugins, https://github.com/aherbert/GDSC-SMLM (accessed: November 2015).

